Absolute negative refraction and imaging of unpolarized electromagnetic waves by two-dimensional photonic crystals

Xiangdong Zhang
Department of Physics, Beijing Normal University, Beijing 100875, People's Republic of China
(Received 26 July 2004; published 1 November 2004)

Absolute negative refraction regions for *both* polarizations of electromagnetic wave in two-dimensional photonic crystal have been found through both the analysis and the exact numerical simulation. Especially, absolute all-angle negative refraction for *both* polarizations has also been demonstrated. Thus, the focusing and image of unpolarized light can be realized by a microsuperlens consisting of the two-dimensional photonic crystals. The absorption and compensation for the losses by introducing optical gain in these systems have also been discussed.

DOI: 10.1103/PhysRevB.70.205102 PACS number(s): 78.20.Ci, 41.20.Jb, 42.70.Qs

I. INTRODUCTION

Recently there has been a great deal of interest in studying a novel class of media that has become known as the left-handed materials.[1–19] These materials are characterized by simultaneous negative permittivity and permeability. Properties of such materials were analyzed theoretically by Veselago over 30 years ago,[1] but only recently they were demonstrated experimentally.[4,5] As was shown by Vesselago, the left-handed materials possess a number of unusual electromagnetic effects including negative refraction, inverse Snell's law, reversed Doppler shift, and reversed Cerenkov radiation. These anomalous features allow considerable control over light propagation and open the door for new approaches to a variety of applications.

It was shown that the negative refraction could also occur in photonic crystal (PC).[20–32] In these PC structures, there are two kinds of cases for negative refraction occuring. The first is the left-handed behavior as being described above.[20–26] In this case, $\vec{k}$, $\vec{E}$ and $\vec{H}$ form a left-handed set of vectors (i.e., $\vec{S}\cdot\vec{k}<0$, where $\vec{S}$ is the Poynting vectors). Another case is that the negative refraction can be realized without employing a negative index or a backward wave effect.[27–32] In this case, the PC is behaving much like a uniform right-handed medium (i.e., $\vec{S}\cdot\vec{k}>0$). In particular, Luo *et al.*[27] have shown that all-angle negative refraction (AANR) could be achieved at the lowest band of two-dimensional (2D) PC. The advantages of negative refraction in the lowest valence band are the single-beam propagation and high transmission efficiency. These can help us to design microsuperlens and realize the focusing of the wave. Very recently, the focusing and the image by 2D PC slab have been demonstrated experimentally.[28–30]

It is well known that the electromagnetic (EM) wave can be decomposed into *E* polarization (*S* wave) and *H* polarization (*P* wave) modes for the 2D PC structures.[33] However, the above discussions about the negative refraction and the focusing of the wave in the 2D PC all focused on a certain polarized wave, *S* wave or *P* wave. It is a natural question to ask whether or not a complete negative refraction region for all polarized waves exists? It is obviously very interesting that the absolute negative refraction region can be found and the focusing of both polarized waves be realized in the 2D PC at the same time. In this paper, we will demonstrate that the complete negative refraction regions for all polarizations exist in some 2D metallodielectric PC structures. Especially, the absolute AANR has also been found. Thus, the focusing and image of unpolarized light can be realized by a microsuperlens consisting of the 2D PC.

The rest of this paper is arranged as follows. In Sec. II, we demonstrate the absolute all-angle negative refraction behaviors in 2D PC. The imaging behaviors for both polarized waves are discussed in Sec. III A conclusion is given in Sec. IV.

II. ABSOLUTE NEGATIVE REFRACTION IN 2D PC

We first consider a 2D square lattice of coated cylinders immersed in a air background with lattice constant a. The coated cylinders have metallic cores coated with a dielectric coating. The radii of metallic core and coated cylinder are $0.15a$ and $0.45a$, respectively. The dielectric constant of dielectric coating is taken as 14, which can be realized by a mixture of glass spheres and alumina flake.[27] For the metallic component, we use the frequency-dependent dielectric constant, $\epsilon=1-[f_p^2/f(f+i\gamma)]$. For all numerical calculations carried out in this work, following Ref. 34, we have chosen $f_p=3600$ THz and $\gamma=340$ THz, which corresponds to a conductivity close to that of Ti. However, our discussions and conclusions given below can apply to other metal parameters as well. In order to simplify the problem, we first consider the cases without absorption ($\gamma=0$). The effect of absorption will be discussed at the latter part. The band structures of this system for the *S* wave and the *P* wave are calculated by the multiple-scattering Korringa-Kohn-Rostoker method. The method has been described in Ref. 35. The results are shown in Fig. 1. Solid curves are for the *P* wave and dotted curves for the *S* wave. We focus on the problems of wave propagation in the low frequency band. Owing to the strong scattering effects, it is generally difficult to describe the propagation behavior of the EM wave in the PC in a simple

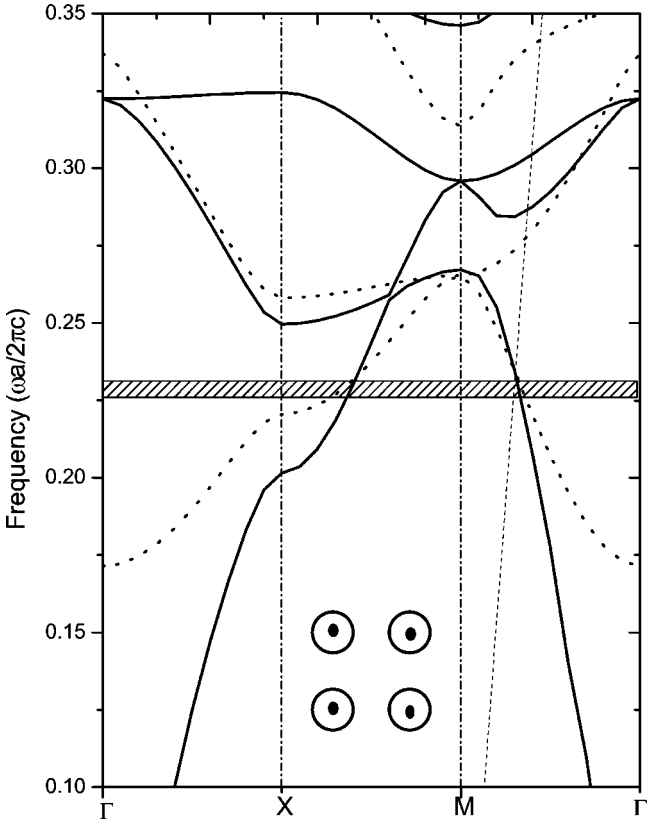

FIG. 1. The calculated photonic band structures of a square lattice of coated cylinder in air for *S* wave (dashed lines) and *P* wave (solid lines). The radii of the dielectric cylinder with $\epsilon=14$ and inner metallic cylinder are $R=0.45a$ and $r=0.15a$, respectively. The light line shifted to *M* is shown by the dashed line. The shadow represents the AANR region. The inset shows the microstructure.

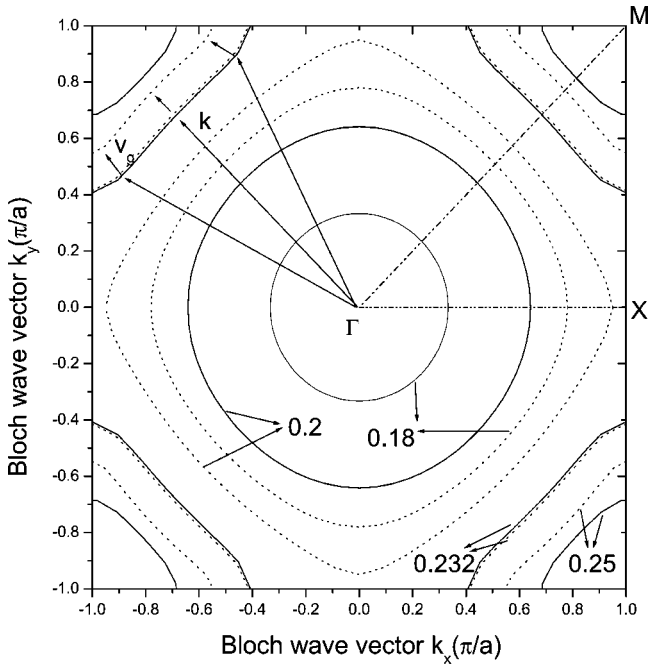

FIG. 2. Several constant-frequency contours for *S* wave (solid lines) and *P* wave (dotted lines) of the first band of the 2D coated PC. The structure and parameters of the PC are identical to those in Fig. 1. The numbers in the figure mark the frequencies in unit of $2\pi c/a$.

yet accurate way. However, a lot of theoretical and experimental practices[20–22,25,27,31,32] have shown that the overall behavior of the wave propagation within a PC can be well described by analyzing the equifrequency surface (EFS) of the band structures, because the gradient vectors of constant-frequency contours in *k* space give the group velocities of the photonic modes. Thus, the propagation direction of energy velocity of the EM wave can be deduced from them. The EFS of the above system can also be calculated by using the multiple-scattering Korringa-Kohn-Rostoker method.[35] The EFS contours for the *S* wave and the *P* wave at several relevant frequencies are demonstrated in Fig. 2.

It is clear from the figures that the lowest bands have $\vec{S}\cdot\vec{k}>0$ everywhere within the first Brillouin zone, meaning that the group velocities (v_g) are never opposite to the phase velocity. Some low frequency contours such as 0.18 and 0.2 are very close to a perfect circle, and the group velocity at any point of the contour is collimated with the *k* vector, indicating that the crystal behaves like an effective homogeneous medium at these long wavelengths. However, the 0.232 contours for both of the *S* wave and the *P* wave are significantly distorted from a circle, which are convex around *M* points. The conservation of the *k* component along the surface of refraction would result in the negative refraction effect in this case. More interestingly, the EFS contours for the *S* wave and the *P* wave at this frequency are basically the same, which leads to the appearance of negative refraction for both polarized waves at the same time. It is valuable to design a frequency region in the 2D PC to realize the negative refraction for both polarized waves. We call such a region as *absolute negative refraction region*. Within this region, some frequencies (shadow region in Fig. 1) are below $0.5\times 2\pi c/a_s$ (where a_s is the surface-parallel period). According to the analysis approach of Ref. 27, we find that they satisfy the required condition for all-angle negative refraction (AANR). Under these conditions, a EM beam incident on the ΓM surface with various incident angle will couple to a single Bloch mode that propagates into this crystal on the negative side of the boundary normal. We define a frequency region for the AANR by using these criteria according to Ref. 27. The shadow region [width 2.5% around $\omega=0.232(2\pi c/a)$] in the Fig. 1 represents such a common region for *both* polarizations of EM wave (*S* wave and *P* wave). We call it *absolute AANR region*. In this region, a slit beam of *S* wave and *P* wave incident on the ΓM surface with various incident angle will propagate into this crystal on the negative refraction side at the same time.

In order to test the above analysis, we do numerical simulations in the present systems. We take the slab samples which consist of 15-layer coated cylinders in the air background with square arrays. The parameters of coated cylinders are the same as the case in Fig. 1. The shape of the

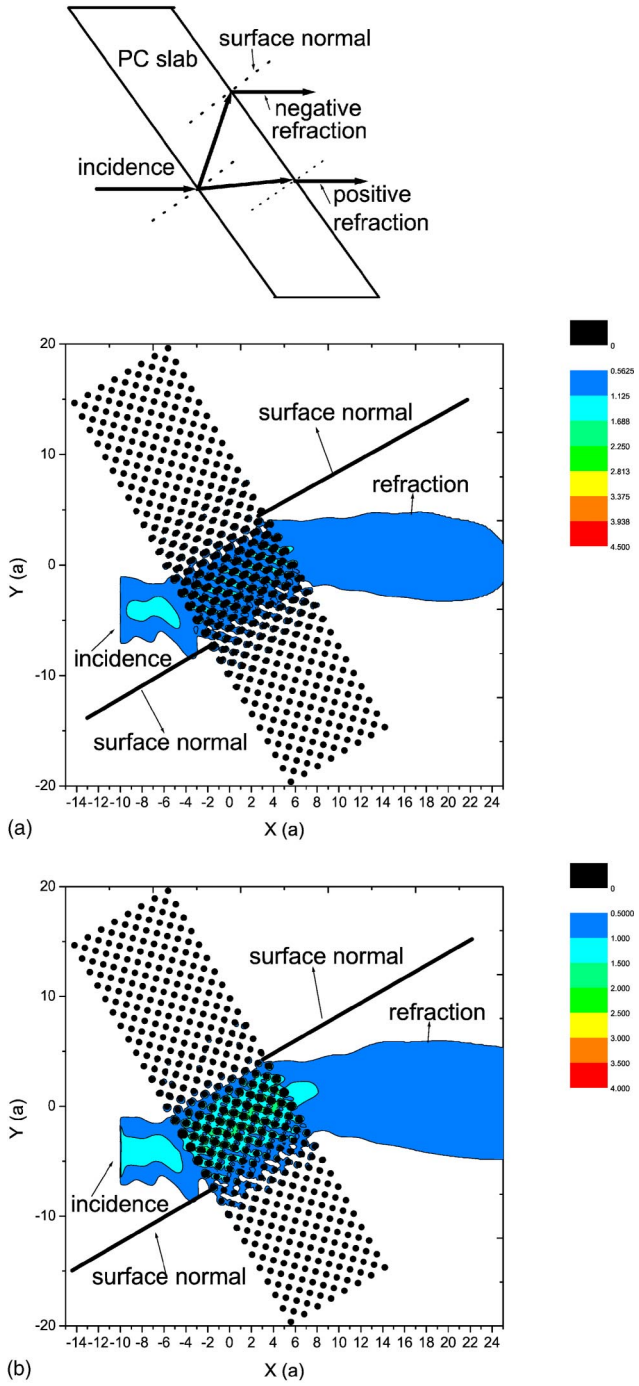

FIG. 3. (Color online) Simulation of negative refraction. The shape of the sample and a snapshot of refraction process are shown on top of the figure. The intensities of electric field for *S* wave (a) and magnetic field for *P* wave (b) for incidence and refraction are shown. The 2D PC slabs with 15-layer thickness are marked as dark dots in the figure. The frequencies of incident wave are $\omega=0.232(2\pi c/a)$ for both polarized waves. The crystal and parameters are identical to those in Fig. 1.

sample and a snapshot of refraction process are shown on the top of Fig. 3. The black frame marks the size of the sample. The surface of the sample is the (11) surface. When a slit beam of frequency $\omega=0.232(2\pi c/a)$ with a half-width $3a$ incident normal to the left surface of the sample, it

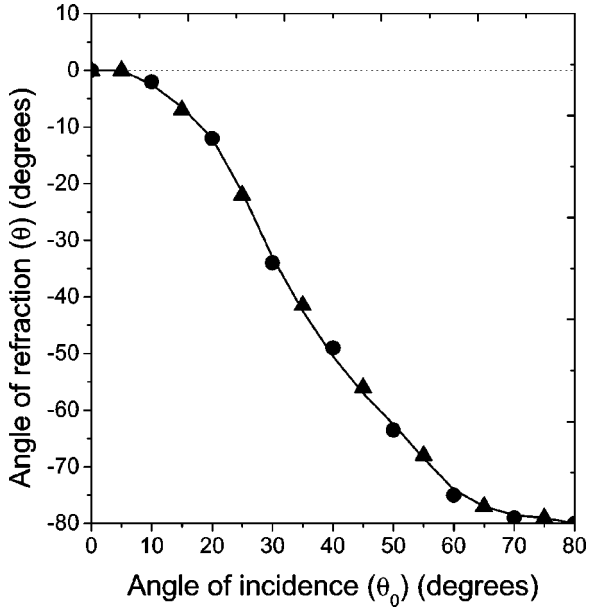

FIG. 4. The angles of refraction (θ) versus angles of incidence (θ_0) at $\omega=0.232(2\pi c/a)$. Circle dots are corresponded to the *S* wave and triangular dots to the *P* wave. The crystal and parameters are identical to those in Fig. 3.

will be refracted two times by two interfaces of the slab. There are two kinds of possibility for the refracted wave. It may be travel on the path of positive refraction or the path of negative refraction as shown in the figure. The simulations are based on a highly efficient and accurate multiple-scattering method.[35] In our simulations, the widths of the samples are taken enough large, such as $40a$, to avoid the edge diffraction effects. The simulation results for the *P* wave and the *S* wave are plotted in Figs. 3(a) and 3(b), respectively. The field energy patterns of incidence and refraction are shown in the figures. The arrows and texts illustrate the various beam directions. It can be clearly seen that the energy fluxes of refraction wave outside of the sample travel on the path of negative refraction. From the directions of refraction energy flux, we can obtain the refraction angle and further refraction index. For example, the refraction angles under the above case at $\omega=0.232(2\pi c/a)$ are about 35° for both polarized waves, which are consistent with the estimation from the EFS in Fig. 2. Then, using Snell's law, we obtain the effective refraction indexes of −0.872. Varying the shape of wedge sample, we have checked the case with different incident angle. Figure 4 shows the refracted angle θ versus incident angle θ_0 at $\omega=0.232(2\pi c/a)$ for the *S* wave (circle dots) and the *P* wave (triangular dots), respectively. Apart from a small region of zero refracted angle corresponding to the small incidence angles, all-angle negative refraction can be observed for both polarized waves at this frequency. Since we know the optimum frequency for a broad angle negative refraction, we can use our PC to test the microsuperlens effect.

III. IMAGING OF UNPOLARIZED ELECTROMAGNETIC WAVE

It is well known that an important application of negative refraction materials is the microsuperlens.[3] Ideally, such a

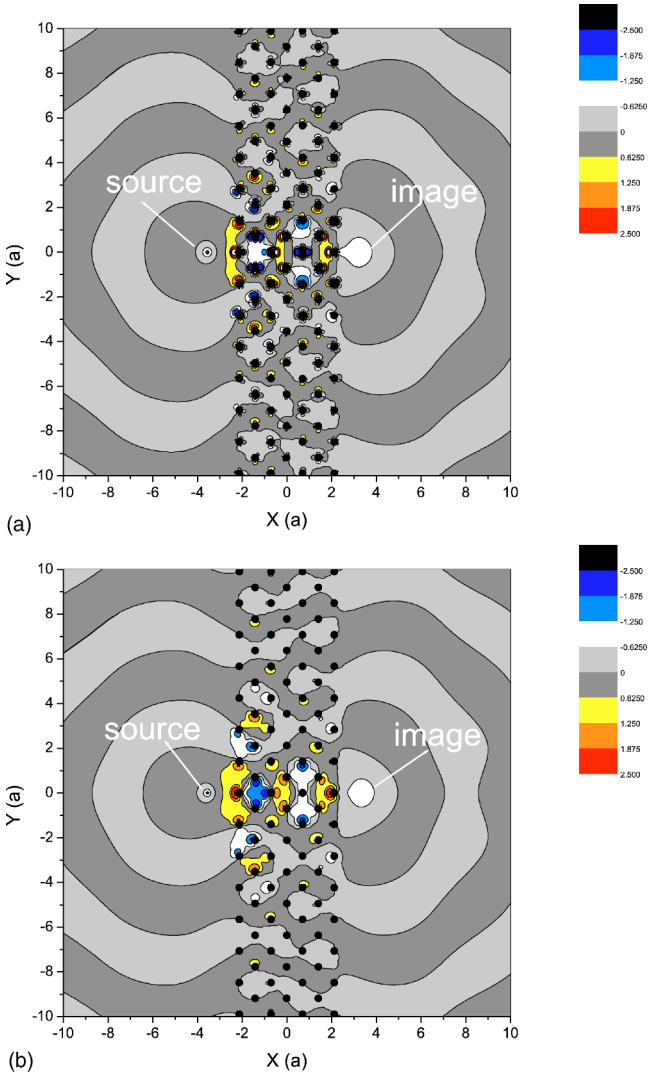

FIG. 5. (Color online) E_z field patterns for S wave (a) and H_z field patterns for P wave (b) of point sources and their images across a seven-layer 2D photonic crystal slab at frequency $\omega=0.231(2\pi c/a)$. The parameters for cylinders are identical to those in Fig. 3. Dark and bright regions correspond to negative and positive E_z (or H_z), respectively.

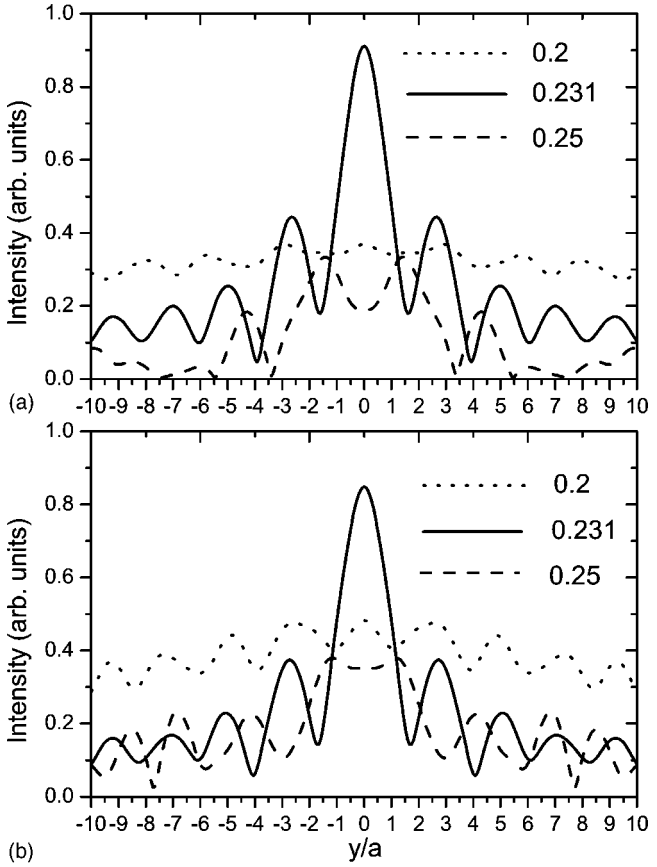

FIG. 6. Intensity distribution for S wave (a) and P wave (b) along the transverse (y) direction at the image plane for several frequencies shown as insets. The crystal and parameters are identical to those in Fig. 5.

superlens can focus a point source on one side of the lens into a real point image on the other side even for the case of a parallel sided slab of material. However, all discussions about the imaging by 2D PC microsuperlens had focused on a certain polarized wave, S wave or P wave. A image of unpolarized light source had not been realized. Based on the knowledge of the absolute negative refraction, in the following, we will explore the possibility to realize such a image.

In order to model such a superlens, we take a slab of the sample with $40a$ width and seven-layer thickness. A continuous-wave point source is placed at a distance $1.0a$ from the left surface of the slab. The frequency of the incident wave emitting from such a point source is $0.231(2\pi c/a)$, chosen to lie within the region where absolute all-angle negative refraction may occur (see Fig. 1). We still employ the multiple-scattering method to calculate the propagation of both polarized waves in such a system. The typical results of E_z field pattern for the S wave and H_z field pattern for the P wave across the slab sample are plotted in Figs. 5(a) and 5(b), respectively. X and Y present vertical and transverse direction of wave propagating, respectively. The fields in the figures are over $20a \times 20a$ region around the center of the sample. The geometries of the PC slab are also displayed. One can find quite a high quality image formed in the opposite side of the slab. A closer look at the data reveals a transverse size (full size at half-maximum) of the image spot as $0.9a$ (or 0.21λ) for the S wave and $0.85a$ (or 0.2λ) for the P wave. In particular, the positions of the image for both polarized waves are approximately the same. They are almost at a distance of $1.0a$ from the right surface of the slab. That is to say, the image of unpolarized wave point source can be realized by such a 2D PC slab.

Our calculations indicate that the high quality images for the unpolarized wave can be obtained only in some certain frequency regions, *absolute AANR region* (shadow region in Fig. 1). The physical reason can be understood by the analysis of Lou *et al.*[31] In order to show this feature, we have plotted the intensity distributions of the S wave and the P wave along the transverse direction (y/a) at the image plane for several frequencies in Figs. 6(a) and 6(b), respectively. Solid lines in figures represent the case

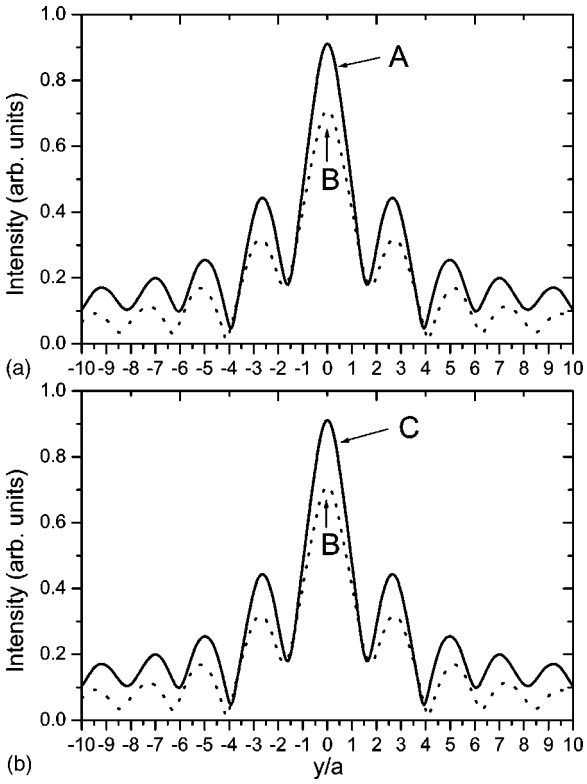

FIG. 7. Intensity distribution along the transverse (y) direction at the image plane. (a) The case with absorption (B) and that without absorption (A). (a) The case with absorption (B) and that with absorption and gain (C). The crystal and parameters are identical to those in Fig. 5.

with $\omega=0.231(2\pi c/a)$ (in the absolute AANR region). The good focusing effects for both polarized waves are clearly visible at this case. With increasing or decreasing the excitation frequencies of the monochromatic sources, and going beyond the absolute AANR region such as dotted, dashed, and dotted-dashed lines in Figs. 6(a) and 6(b), we find that the focusing effects degrade gradually and disappear at the end.

The above discussion only focused on one kind of metallodielectric system. In fact, a few other systems also possess similar character, such as some systems of coated cylinder with internal metal cylinder coated by semiconductor Ge ($\epsilon=18$) in air background. The common feature of these systems is that they all include metal component. Therefore, the absorption for these systems is inevitable. Lou *et al.*[31] have pointed out that the central image peak disappears and the image degrades gradually with the increase of absorption. However, fortunately, the loss can be overcome by introducing the optical gain in the systems. Recently, Ramakrishna and Pendry[16] have suggested a method to remove the absorption by introducing optical gain into the lens made from a multilayers stack of thin alternating layers of silver and dielectric medium. Here, we borrow their idea and introduce the optical gain in the 2D PC superlens. Because it is not sensitive to the absorption and the gain for the P wave in the present system, we only present the calculated results for the S wave. Figure 7(a) shows the intensity distribution as a function of transverse coordinate (y/a) for the S wave at the image plane ($1.0a$ away from the second interface). Curve A is corresponded to the case without absorption and curve B to that with absorption, in this case γ is taken as 340 THz. Comparing curve A with curve B, we find that the central peak of the image decreases with the introduction of absorption, which is in agreement with the analysis of Ref. 31. The result by introducing gain to remove the absorption for the corresponding case is plotted in Fig. 7(b). Curves B in Figs. 7(a) and 7(b) are the same, and curve C in Fig. 7(b) is the result with the dielectric constant $\epsilon=14-0.12i$ for the dielectric part of the coated cylinder. We do not find any difference between curve A in Fig. 7(a) and curve C in Fig. 7(b). In fact, for any case of absorption, the loss can always be compensated by introducing the fitted gain. Thus, the lens based on the above 2D PC can work well even in the presence of absorption. We would like to point out that the optical gains being introduced are small and they cannot let the system reach the threshold of lasing. Thus, no lasing solutions can be produced in the present cases. The optical gain here only plays a role on improving the wave intensity.

IV. CONCLUSION

Based on the exact numerical simulations and physical analysis, we have found the absolute negative refraction regions for *both* polarizations of EM wave in the 2D PC. Especially, the absolute all-angle negative refraction for *both* polarizations has also been demonstrated. The focusing and image of unpolarized light have been obtained by a microsuperlens consisting of the 2D PC. Although the losses due to the absorption reduce the intensity of the central peak of the image, it can always be compensated by introducing fitted optical gain in these systems. Therefore, the lens based on the 2D PC is applicable even in the presence of absorption. We hope that this work can stimulate the interests of experimental studies of focusing and image of unpolarized light in the 2D PC.

ACKNOWLEDGMENTS

The authors wish to thank C. T. Chan for useful discussion. This work was supported by the National Natural Science Foundation of China (Grant No. 10374009) and the National Key Basic Research Special Foundation of China under Grant No. 2001CB610402. The project sponsored by SRF for ROCS, SEM and the Grant from Beijing Normal University.

[1] V. G. Veselago, Sov. Phys. Usp. **8**, 2854 (1967) [Sov. Phys. Usp. **10**, 509 (1968)].
[2] J. B. Pendry, A. J. Holden, D. J. Robbins, and W. J. Stewart, IEEE Trans. Microwave Theory Tech. **47**, 2075 (1999).
[3] J. B. Pendry, Phys. Rev. Lett. **85**, 3966 (2000).
[4] D. R. Smith, W. J. Padilla, D. C. View, S. C. Nemat-Nasser, and S. Schultz, Phys. Rev. Lett. **84**, 4184 (2000); D. R. Smith and N. Kroll, *ibid.* **84**, 2933 (2000).
[5] R. A. Shelby, D. R. Smith, and S. Schultz, Science **292**, 77 (2001).
[6] P. Markos and C. M. Soukoulis, Phys. Rev. E **65**, 036622 (2002); Phys. Rev. B **65**, 033401 (2002).
[7] Focus issue, Opt. Express, **11**, 7 (2003).
[8] G. Shvets, Phys. Rev. B **67**, 035109 (2003).
[9] V. A. Podolskiy, A. K. Sarychev, and V. M. Shalaev, Opt. Express **11**, 735 (2003).
[10] S. Foteinopoulou, E. N. Economou, and C. M. Soukoulis, Phys. Rev. Lett. **90**, 107402 (2003).
[11] J. Pacheco Jr., T. M. Grzegorczyk, T. B. I. Wu, Y. Zhang, and J. A. Kong, Phys. Rev. Lett. **89**, 257401 (2002).
[12] Y. Zhang, B. Fluegel, and A. Mascarenhas, Phys. Rev. Lett. **91**, 157404 (2003).
[13] D. R. Smith and D. Schurig, Phys. Rev. Lett. **90**, 077405 (2003).
[14] A. A. Houck, J. B. Brock, and I. L. Chuang, Phys. Rev. Lett. **90**, 137401 (2003); C. G. Parazzoli *et al.*, *ibid.* **90**, 107401 (2003).
[15] J. Li, L. Zhou, C. T. Chan, and P. Sheng, Phys. Rev. Lett. **90**, 083901 (2003).
[16] S. A. Ramakrishna and J. B. Pendry, Phys. Rev. B **67**, 201101(R) (2003).
[17] R. Merlin, Appl. Phys. Lett. **84**, 1290 (2004).
[18] A. Grbic and G. V. Eleftheriades, Phys. Rev. Lett. **92**, 117403 (2004).
[19] A. N. Lagarkov and V. N. Kissel, Phys. Rev. Lett. **92**, 077401 (2004); L. Chen, S. He, and L. Shen, *ibid.* **92**, 107404 (2004).
[20] H. Kosaka, T. Kawashima, A. Tomita, M. Notomi, T. Tamamura, T. Sato, and S. Kawakami, Phys. Rev. B **58**, R10 096 (1998).
[21] M. Notomi, Phys. Rev. B **62**, 10 696 (2000).
[22] B. Gralak, S. Enoch, and G. Tayeb, J. Opt. Soc. Am. A **17**, 1012 (2000).
[23] C. Luo, M. Ibanescu, S. G. Johnson, and J. D. Joannopoulos, Science **299**, 368 (2003).
[24] E. J. Read, M. Soljacic, and J. D. Joannopoulos, Phys. Rev. Lett. **91**, 133901 (2003).
[25] S. Foteinopoulou and C. M. Soukoulis, Phys. Rev. B **67**, 235107 (2003).
[26] P. V. Parimi, W. T. Lu, P. Vodo, J. Sokoloff, J. S. Derov, and S. Sridhar, Phys. Rev. Lett. **92**, 127401 (2004).
[27] C. Luo, S. G. Johnson, J. D. Joannopoulos, and J. B. Pendry, Phys. Rev. B **65**, 201104(R) (2002); Opt. Express **11**, 746 (2003); C. Luo, S. G. Johnson, and J. D. Joannopoulos, Appl. Phys. Lett. **83**, 2352 (2002).
[28] E. Cubukcu, K. Aydin, E. Ozbay, S. Foteinopoulou, and C. M. Soukoulis, Nature (London) **423**, 604 (2003).
[29] P. V. Parimi, W. T. Lu, P. Vodo, and S. Sridhar, Nature (London) **426**, 404 (2003).
[30] E. Cubukcu, K. Aydin, E. Ozbay, S. Foteinopoulou, and C. M. Soukoulis, Phys. Rev. Lett. **91**, 207401 (2003).
[31] C. Luo, S. G. Johnson, J. D. Joannopoulos, and J. B. Pendry, Phys. Rev. B **68**, 045115 (2003).
[32] Z. Y. Li and L. L. Lin, Phys. Rev. B **68**, 245110 (2003).
[33] J. D. Joannopolous, R. D. Meade, and J. N. Winn, *Photonic Crystals* (Princeton University, Princeton, NJ, 1995).
[34] M. M. Sigalas, C. T. Chan, K. M. Ho, and C. M. Soukoulis, Phys. Rev. B **52**, 11 744 (1995); L. M. Li, Z. Q. Zhang, and X. Zhang, Phys. Rev. B **58**, 15 589 (1998).
[35] L. M. Li and Z. Q. Zhang, Phys. Rev. B **58**, 9587 (1998); X. Zhang, Z. Q. Zhang, L. M. Li, C. Jin, D. Zhang, B. Man, and B. Cheng, *ibid.* **61**, 1892 (2000).